A Stable Quaternized Chitosan-Black Phosphorus Nanocomposite for Synergetic Disinfection of Antibiotic-Resistant Pathogens

Yi Zhang,* Xu-Fang Qu, Cheng-Long Zhu, Han-Jie Yang, Chen-Hui Lu, Wen-Long Wang, Yuehong Pang, Cheng Yang, Li-Jian Chen, and Xing-Fang Li

Cite This: *ACS Appl. Bio Mater.* 2021, 4, 4821–4832
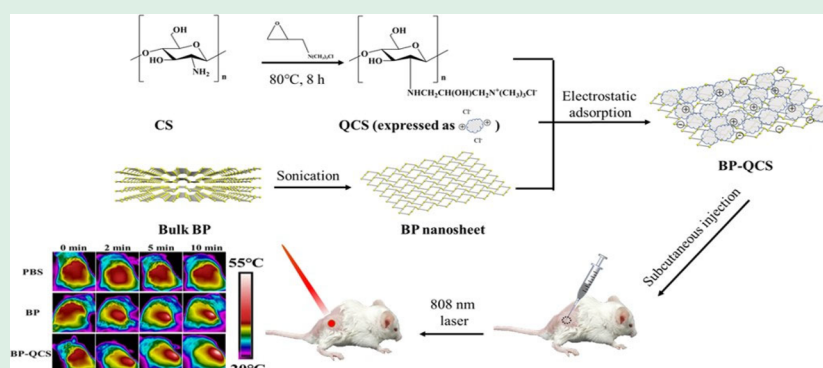
Read Online

ACCESS | Metrics & More | Article Recommendations | Supporting Information

ABSTRACT: Antibiotics are widely used for treatment of bacterial infections, and their overuse has contributed to microbial resistance. Currently, an alternative antibiotic-free therapy for inactivating bacteria is of great interest. Black phosphorus (BP), a biocompatible and nontoxic rising-star two-dimensional layered material, has gained remarkable interest in many bioapplications including biosensing, cancer therapy, drug delivery, and also antibacterial treatment. However, BP nanosheets suffer from instability in ambient environments due to rapid oxidation and degradation. To address this issue, BP nanosheets were modified with quaternized chitosan (QCS) by electrostatic adsorption to prepare a BP-QCS composite for photothermal/pharmaco treatment of bacterial infection. The BP-QCS has obviously enhanced solubility and chemical stability in aqueous suspensions. We have demonstrated that under near-infrared (NIR) irradiation, the BP-QCS can synergistically inactivate more than 95% methicillin-resistant *Staphylococcus aureus* (*S. aureus*) (MRSA) and *Escherichia coli* within 10 min with a dose of only 75 μg/mL in vitro. Meanwhile, the BP-QCS composite under NIR can synergistically inactivate 98% *S. aureus* in vivo. Furthermore, the BP-QCS suspensions at effective antibacterial concentrations have negligible cytotoxicity and in vivo toxicity.

KEYWORDS: black phosphorus, stability, quaternized chitosan, photothermal disinfection, antibacterial activity

■ INTRODUCTION

The inappropriate use of antibiotics has increased the number of medication-resistant germs, and particularly, this has even led to problems with hospital-acquired infections, with respect to both increased incidence and cost.[1,2] The emergence of drug-resistant bacteria is much faster than developing a new drug. For these reasons, developing antibiotic-free medicines and treatments is imperative so that bacteria will not develop resistance.[3]

Photothermal therapy is an alternative method in which tissues are ablated by heat generated from absorbed light energy.[4−6] In recent years, it has been used in the treatment of tumors and bacterial infection.[7−9] Near-infrared (NIR) is preferred over visible light for in vivo photothermal therapy because of its better penetrating ability to reach the target position through tissues.[10,11] Graphene,[12,13] ternary chalcogenide Ta$_2$NiS$_5$-P nanosheets,[14] molybdenum disulfide nano-

sheets,[4,15] gold nanomaterials,[16] metal−organic frameworks,[17] and organic dyes[18] have been used for photothermal therapy because of high light-to-heat conversion efficiency.

Black phosphorus (BP) nanosheets have recently attracted attention because of their tunable, extensive absorption ranged from the UV to NIR region, good biocompatibility, reactive oxygen species (ROS) generation, and photothermal conversion efficiency.[19,20] BP has been applied in many bioapplications including biosensing,[21] neuroprotective nanomedicine,[22] drug delivery,[23] biomineralization,[24] cancer

Scheme 1. Schematic Illustration of the Synthesis of BP-QCS and the Disinfection Treatment with the Synergetic Antibacterial Effect
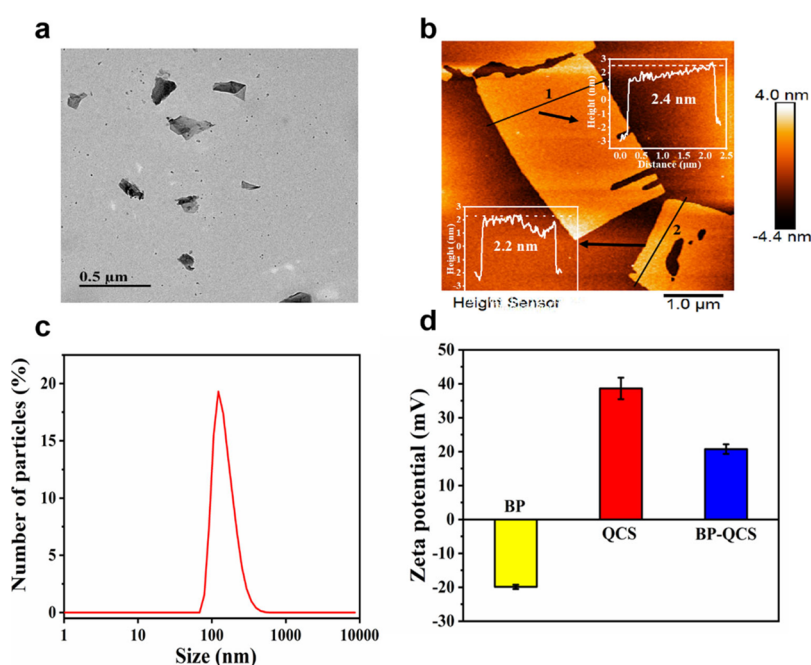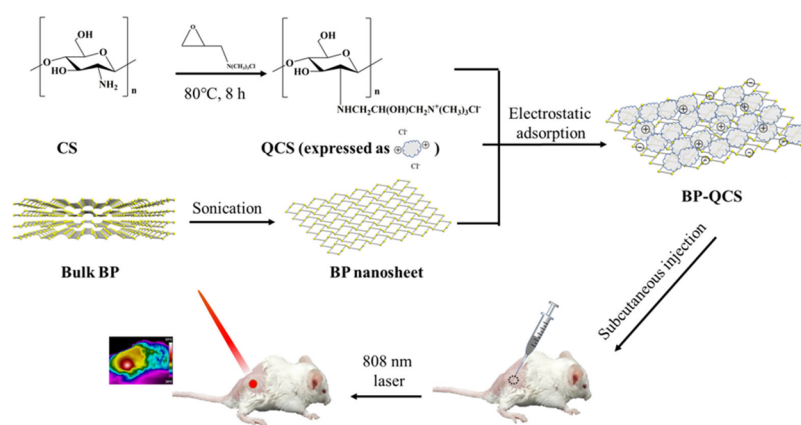

Figure 1. (a) TEM image of BP nanosheets. (b) AFM image of BP nanosheets. (c) Hydrodynamic size of BP nanosheets. (d) Zeta potential of BP, QCS, and BP-QCS.

therapy,[25−27] pathogen capture and release,[28] and also disinfection.[29] Chen et al. demonstrated that BP nanosheets can protect neuronal cells from Cu^{2+}-induced neurotoxicity by capturing Cu^{2+} selectively and efficiently and improve the blood−brain barrier permeability under NIR laser irradiation due to their strong photothermal effect.[22] Guo et al. found that BP nanosheets killed both Gram-negative and Gram-positive bacteria with a concentration and time-dependent antibacterial activity.[30] The main antibacterial mechanism was considered as physical damage to the bacterial membrane (caused by sharp edges of BP nanosheets) and RNA leakage. Liu et al. reported that chemically degradable BP nanosheets can function as antibacterial agents by producing of ROS under visible-light irradiation.[31] To achieve enhanced disinfection activity by promoting ROS photogeneration, several BP nanocomposites, such as BP/Ag nanocomposites,[29,32] BP/Cu nanocomposites,[33] and BP/graphitic carbon nitride,[34] have been developed. Besides inducing the production of ROS, photothermal conversion is another important mechanism of BP-

based disinfection. Aksoy et al. synthesized BP/Au nanocomposites and investigated the photothermal antibacterial and antibiofilm activities against a pathogenic biofilm-forming bacterium under NIR light irradiation.[35] The bacterial cell membrane was destructed by BP/Au more efficiently than by bare BP or Au due to the higher photothermal conversion efficiency of BP/Au nanocomposites.

However, BP tends to react with adsorbed water or oxygen on its surface resulting in poor stability in ambient, which affects its storage and thus limits its potential as a drug.[36] Surface coordination or chemical modification of BP by natural organic antibacterial molecules may help to improve its stability, bacteria-targeted ability, and antibacterial efficiency because of a photothermal/pharmaco synergetic strategy. BP nanosheets have so far been modified with a titanium aminobenzenesulfanato complex (a weak antibacterial agent),[37] poly(4-pyridonemethylstyrene) endoperoxide to control the storage and release of ROS reversibly,[38] and a thermal-sensitive liposome to release pharmaceuticals in a
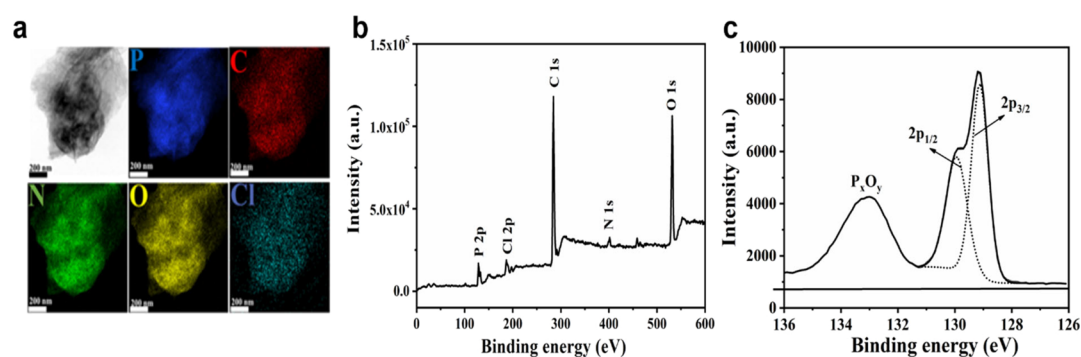
Figure 2. (a) STEM image of BP-QCS and the elemental mapping of P, C, N, O, and Cl. (b) XPS spectrum of BP-QCS. (c) Peak fitting graph of the P element.
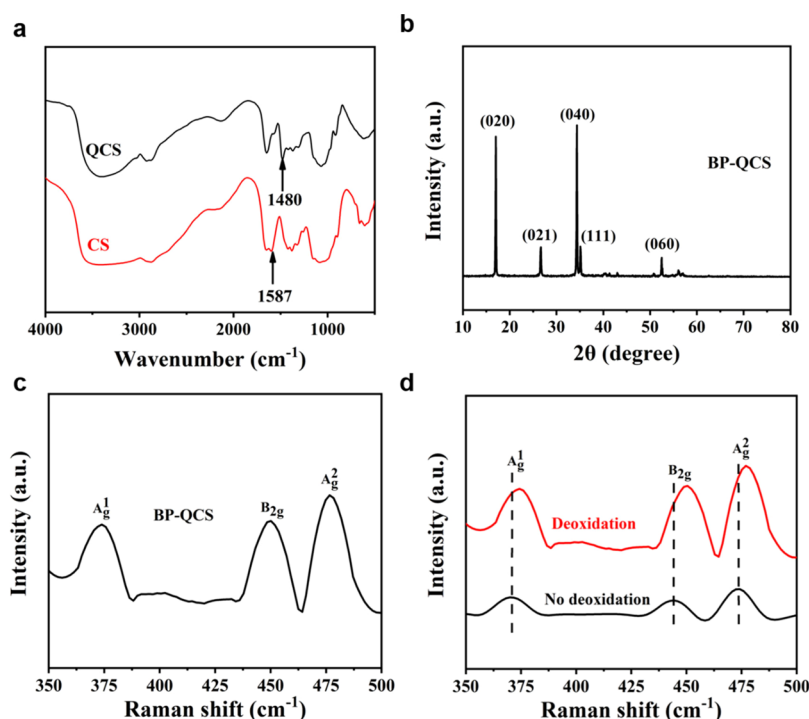

Figure 3. (a) FTIR spectra of CS and QCS. (b) XRD of BP-QCS. (c) Raman spectra of BP-QCS. (d) Raman spectrum of BP nanosheets prepared under conditions with or without deoxidation.

spatial-, temporal-, and dosage-controlled fashion.[39] The antibacterial mechanism was reported as that the nanocomposite induced bacterial inactivation via membrane depolarization, suppression of protein synthesis, and decomposition of genome DNA.

Chitosan (CS) is an abundant natural antibacterial agent and is widely used in the treatment of bacterial infections because it is highly biocompatible and harmless to humans.[40−43] However, it can only be dissolved in acids, not in a neutral aqueous solution, limiting its use as a hydrogel to promote healing of superficial wounds[44] or as a filtration membrane for water disinfection.[45] Another problem is its low antibacterial efficiency when working alone. Therefore, we propose to improve its solubility and antibacterial ability by modification of CS.

In this study, we have synthesized quaternized chitosan (QCS) by modifying CS with quaternary ammonium and prepared the BP-QCS nanocomposite by electrostatically adsorbing QCS onto BP nanosheets acquired via ultrasonication-assisted aqueous-phase exfoliation (Scheme 1).

The BP-QCS nanocomposite was much more dispersive and chemically stable than BP in aqueous solution. In vitro and in vivo antibacterial tests showed that the synthesized BP-QCS has good biocompatibility and photothermal/pharmaco synergetic antibacterial activity under NIR irradiation and is expected to have potential applications in antibacterial treatment.

■ RESULTS AND DISCUSSION

Preparation and Characterization of BP-QCS. Bulk BP was subjected to ultrasonication in pure water, and freestanding few-layer BP nanosheets with flake structures were obtained by ultrasonication-assisted aqueous-phase exfoliation. They exhibit typical 2D morphology with lateral size of a few hundred nanometers and a thickness of ~4 nm, corresponding to 2 to 4-layer BP nanosheets (Figure 1a,b). DLS analysis shows that the hydrodynamic size of these BP nanosheets ranges from tens to several hundred nanometers, with an average size of 212 nm (Figure 1c). There are strong intralayer
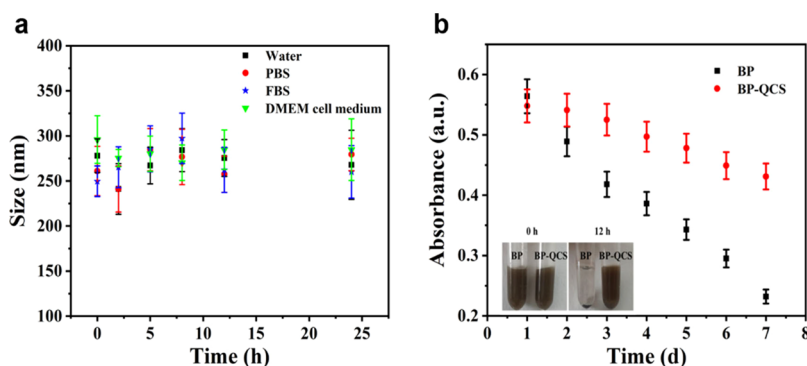
Figure 4. Stability performance of BP-QCS and BP. (a) Hydrodynamic size of BP-QCS for 24 h in water, PBS, FBS, and DMEM cell media. (b) Absorption decay at 808 nm of BP nanosheets and BP-QCS for 7 days (the inset shows the corresponding photographs of BP and BP-QCS for 0 and 12 h).

P−P bonds and weak van der Waals forces between the layers in BP materials. Bulk BP could be turned into few-layer or even single-layer BP nanosheets by breaking van der Waals forces using liquid-phase exfoliation.[44,46,47] Although BP can be exfoliated more efficiently assisted by amide solvents such as N,N-dimethylformamide and N-methyl pyrrolidone, it is very difficult to remove the adsorbed amide solvent molecules completely from the surface of BP, impeding its in vivo applications.[8,48] To obtain clean BP nanosheets, exfoliation in pure water was applied here without using amide solvents, and the product was acceptable in view of the amount, 2D size, and number of layers.

We also examined the absorption spectra of the raw material bulk BP and its product as an additional proof of successful exfoliation because BP materials of different sizes and numbers of layers have different absorbance characteristics. Compared with bulk BP, the as-prepared BP nanosheets have much stronger absorption in the wide wavelength range of 400−850 nm (Figure S1), indicating the successful formation of few-layer BP nanosheets. In addition, the strong absorption of the as-prepared BP nanosheets in the visible and NIR regions would benefit their application in photothermal conversion.

QCS, the modified compound for BP nanosheets, was obtained by quaternizing CS with glycidyltrimethylammonium chloride (GTA), and BP-QCS was synthesized by electrostatic adsorption of QCS onto BP nanosheets. Figure 1d displays the zeta potential of BP nanosheets, QCS, and BP-QCS. The potential of bare BP nanosheets is −19.9 mV. After adsorption of positively charged QCS (+38.6 mV) onto bare BP nanosheets, the potential of BP-QCS becomes +20.7 mV. The electrostatic adsorption of positively charged BP-QCS onto negatively charged bacteria cells would be more efficient.

Figure 2a shows the STEM image and elemental mapping of BP-QCS. The distribution of C, N, O, and Cl from QCS is completely consistent with that of P from BP nanosheets, revealing that QCS is uniformly distributed on the surface of BP nanosheets. The chemical composition of P, C, N, O, and Cl elements measured by X-ray photoelectron spectroscopy (XPS) further confirms the successful adsorption of QCS onto BP nanosheets and the formation of BP-QCS with good purity (Figure 2b). According to high-resolution XPS, BP-QCS shows the typical P 2p$_{3/2}$ (129.5 eV) and P 2p$_{1/2}$ (130.4 eV) doublets of crystalline BP and a broad peak at ∼133 eV corresponding to oxidized phosphorus (i.e., P$_2$O$_4$ or P$_2$O$_5$ moieties) sub-bands, likely stemming from oxygen defects or surface

suboxides in BP that are introduced during exfoliation (Figure 2c).

Figure 3a shows the Fourier transform infrared (FTIR) spectra of both the raw material CS and the product QCS. The decrease of the amino N−H absorption peak intensity at 1587 cm^{-1} and a new methyl absorption peak at 1480 cm^{-1} indicates the successful substitution of some hydrogen atoms in amino groups (−NH$_2$) of CS molecules by GTA. Conductivity titration of chloride ions in QCS found that the substitution degree of CS by quaternization was 56% (Figure S3). The quaternized product QCS was soluble in water, whereas the raw material CS settled to the bottom of the container in minutes, indicating the improved water solubility of QCS after quaternization (Figure S2).

There were five characteristic peaks at 17.2, 26.5, 34.4, 35.1, and 52.3° in the XRD spectrum of BP-QCS, which were indexed to the (020), (021), (040), (111), and (060) planes of BP crystals,[49] respectively (Figure 3b), indicating that the crystal structure of BP remained unchanged after being functionalized with quaternized chitosan. In the Raman spectrum of our product BP-QCS, A$_g^1$ (one out-of-plane vibration mode), B$_{2g}$, and A$_g^2$ (two in-plane vibration modes) of BP nanosheets at wavenumbers of 370.3, 444.7, and 474.6 cm^{-1} were detected, respectively (Figure 3c).

The Raman spectra of BP nanosheets prepared under conditions with or without deoxidation were also compared. The Raman scattering peaks of BP without deoxidation are lower and blueshifted than those of BP with deoxidation, indicating less number of layers and slight degradation in the presence of oxygen (Figure 3d).[50]

Stability of BP-QCS. To investigate the solubility of BP-QCS samples, they were uniformly dispersed in water, fetal bovine serum (FBS), phosphate-buffered saline (PBS), and DMEM cell media under sonication to become a suspension of the same concentration and were kept at room temperature. After 12 h, there were no obvious aggregation and reduction of particle size for BP-QCS, indicating that BP-QCS has good solubility in all of the media that we tested (Figure 4a and Figure S4). It should be noted that we use the content of BP nanosheets to represent the concentration of BP-QCS in this and the following sections.

BP is irreversibly oxidized by oxygen in water easily, forming oxidized phosphorus P$_x$O$_y$, and then converted into the final anion PO$_4^{3-}$.[21,51] Degradation of BP leads to the decrease in its absorbance. The absorption spectra of BP nanosheets and BP-QCS in PBS were then tracked and recorded, in order to know
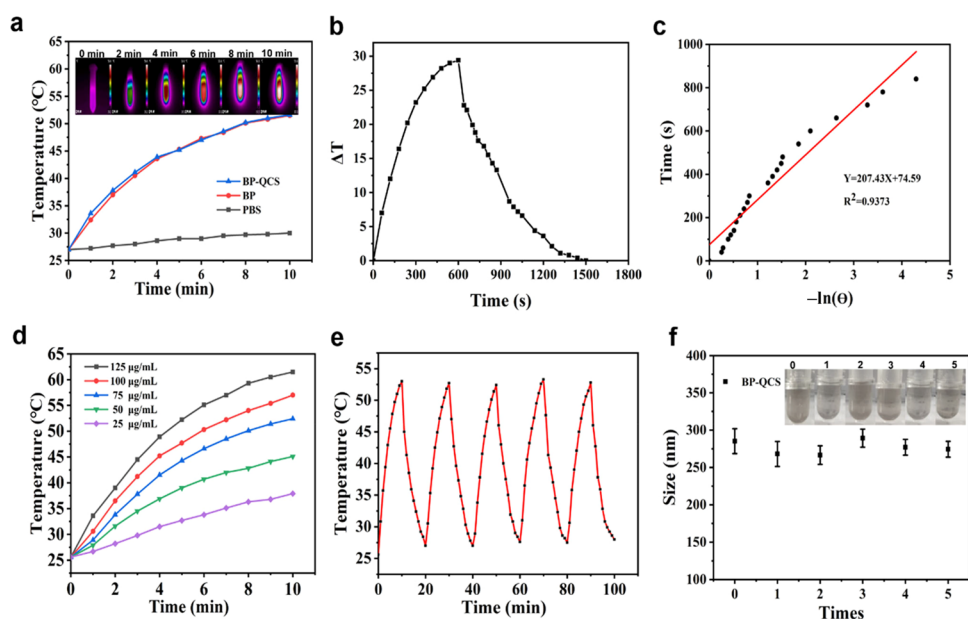
Figure 5. Photothermal properties of BP-QCS. (a) Photothermal curves of PBS, BP nanosheets, and BP-QCS under 808 nm laser irradiation (1 W/cm^2) for 10 min (inset: thermal images of BP nanosheets). (b) Temperature change (ΔT) response to the NIR laser on (0−600 s) and off (600−1500 s). (c) Linear time data versus $-\ln(\theta)$ obtained from the cooling period of the NIR laser off. (d) Photothermal performance of BP-QCS at different concentrations. (e) Photothermal cycle of BP-QCS. (f) Hydrodynamic size of BP-QCS after different times of NIR irradiation, 10 min each time (inset: corresponding photographs of the BP-QCS).
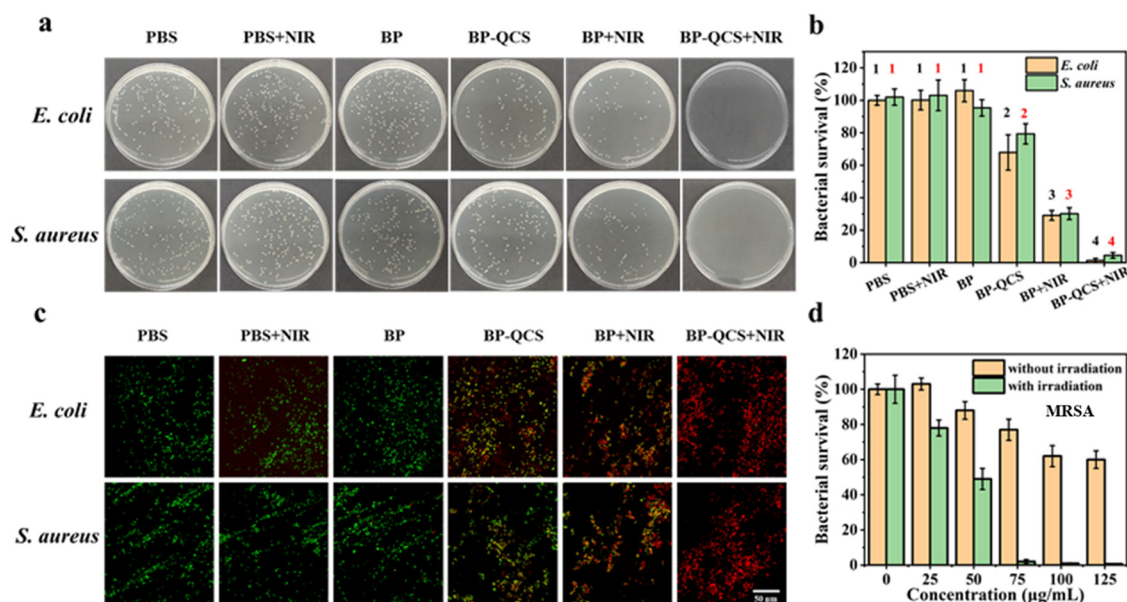

Figure 6. In vitro antibacterial activity. (a) Photographs of agar plates of *E. coli* and *S. aureus* after treatments. (b) Bacterial viability of *E. coli* and *S. aureus* after different treatments. 1−4 indicate that the groups marked with different numbers have significant differences ($p < 0.05$). (c) LIVE/DEAD fluorescence staining of *E. coli* and *S. aureus* after different treatments (scale bar = 50 μm). (d) Survival rates of MRSA at different concentrations of BP-QCS with or without NIR irradiation.

their stability. The absorbance intensity of bare BP nanosheets decreased obviously with increasing storage time, indicating a significant degradation of BP. In contrast, absorbance of BP-QCS was relatively stable, with only a slight decrease. For instance, the absorption of BP at 808 nm decreased by 59% at day 7, whereas that of BP-QCS decreased only by 22%, revealing that BP-QCS has better stability (Figure 4b). The possible reason for the improved stability of BP-QCS is that BP nanosheets are coated with a layer of QCS, which reduces

the contact between BP and oxygen or water, thereby reducing degradation and improving stability.

Photothermal Properties. The photothermal conversion performance of BP and BP-QCS was studied under NIR irradiation (808 nm, 1 W/cm^2, and 10 min). After 10 min of irradiation, the temperature of PBS increased by less than 5 °C, whereas the temperatures of BP nanosheets and BP-QCS suspensions increased by more than 25 °C (Figure 5a). There is no significant difference in the temperature increase between BP nanosheets and BP-QCS suspensions.

The photothermal conversion efficiency (PCE) of BP-QCS was evaluated with the solvent (water) as a negative control. After irradiation with an 808 nm NIR laser at 1 W/cm² for 600 s, the temperature of BP-QCS aqueous dispersions increased to 56.6 °C, and there was a temperature increase of 29.4 °C (Figure 5b). By comparison, the temperature increase of pure water was only 2.3 °C. After the NIR laser was turned off at 600 s, the decreased temperature was recorded for another 900 s. Linear time data versus $-\ln(\theta)$ obtained from the cooling period of the NIR laser is shown in Figure 5c. The photothermal conversion efficiency (η) of BP-QCS can be calculated according to the following equation[52]

$$\eta = \frac{hA(\Delta T_{\max,\mathrm{mix}} - \Delta T_{\max,H_2O})}{I(1 - 10^{-A_\lambda})}$$

where η is the heat transfer coefficient, A is the surface area of the container, $\Delta T_{\max,\mathrm{mix}}$ and $\Delta T_{\max,H_2O}$ are the temperature change of the BP-QCS dispersion and the solvent (water) at the maximum steady-state temperature, respectively, I is the laser power, and A_λ is the absorbance of BP-QCS at 808 nm. According to the equation, the η value and the extinction coefficient (ε) of BP-QCS were calculated to be about 55.7% and 0.53, respectively.

The photothermal effect of BP-QCS is dependent on concentration (Figure 5d). The higher the concentration of BP-QCS, the higher the temperature increases under the same irradiation power and time. The temperature can reach up to 53 °C at 75 μg/mL BP-QCS. After five cycles of irradiation, the temperature could still be raised to 52.8 °C (Figure 5e). After BP was irradiated by NIR irradiation 5 times, the particle size did not change significantly, and there was no obvious precipitation at the bottom of the test tube (Figure 5f). The absorption spectra of BP-QCS almost coincide with each other before and after irradiation, and the color of the solution does not change significantly (Figure S5). All the above results indicate that BP-QCS has good photothermal stability.

In Vitro Antibacterial Activity. After optimization of sterilization time and bactericidal concentration (Figure S6), we used the plate counting method to evaluate the in vitro antibacterial activity of the bare BP nanosheets, QCS, and BP-QCS with or without irradiation of the NIR laser. The PBS group was used as a control to calculate the relative bacterial survival rate. As demonstrated in Figure 6a,b, the bacterial survival rates in PBS, PBS+NIR, and BP groups are about 100%, signifying that BP or NIR alone has no bacteriostatic effect. The bacterial survival rate is decreased by more than 20% after QCS coating of BP nanosheets, indicating improved antibacterial activity of BP nanosheets with QCS, a positively charged chemical prepared from the natural antibacterial agent CS.

We compared the antibacterial performance of CS and QCS as well. As can be seen in Figure S7, CS at a concentration as high as 10 μg/mL did not show obvious antibacterial ability, whereas QCS at 5 μg/mL could inhibit the growth of both *Escherichia coli* (*E. coli*) and *Staphylococcus aureus* (*S. aureus*) by nearly 50%. The antibacterial activity of CS and QCS is due to their bonding with the negatively charged phospholipid groups of cell membranes, which increases membrane permeability and creates more membrane holes, eventually leading to cell death.[53−55] As the membrane of mammalian cells is also negatively charged, the high antibacterial activity of QCS induces unavoidable cytotoxicity against mammalian

cells. As expected, cytotoxicity against mammalian cells considerably increased with an increasing antibacterial ability after CS was quaternized into QCS (Figure S8). In the presence of QCS at 5 μg/mL, the survival rate of the 3T3 cell line was less than 60%. Therefore, it is not ideal to use CS or QCS alone as an antibacterial agent because of their low activity or high cytotoxicity, respectively. The antibacterial activity of BP-QCS against methicillin-resistant *S. aureus* (MRSA) with or without NIR irradiation was measured by agar plate assay, and the corresponding quantitative analysis is shown in Figure 6d. The bacteriostatic effect of BP-QCS with or without NIR light irradiation was enhanced with the increase in BP-QCS concentration. At the same concentration, the bacteriostatic ability of the irradiation group was significantly higher than that of the nonirradiation group. When the concentration of BP-QCS was 75 μg/mL, the inhibitory rate of BP-QCS under NIR light conditions was as high as 98%, and the bacterial growth was completely inhibited when BC-QCS was more than 75 μg/mL, indicating its high antibacterial efficacy against MRSA, the typical drug-resistant bacteria.

Compared with the BP group, whose bacterial survival rates were around 100% for both *E. coli* and *S. aureus*, and the BP-QCS group (*E. coli*, 67.9%; *S. aureus*, 79.3%), the bacterial survival rates of BP+NIR (29.1%; 30.1%) and BP-QCS+NIR (1.3%; 4.4%) groups were much lower, suggesting that photothermal disinfection plays a major role in the synergetic antibacterial effect of the photothermal antibacterial property of BP and the membrane targeting and chemically antibacterial ability of QCS. In addition, the material has a stronger antibacterial ability against *E. coli*, which is due to the thicker cell walls of Gram-positive bacteria.

The cell viability assay was also accomplished by a LIVE/DEAD fluorescence staining method (Figure 6c). Calcein-AM could stain the live cells with green fluorescence after a series of reactions, whereas PI could enter the dead cells through damaged cell membranes and form complexes with the DNA double helix in the nucleus to generate red fluorescence. The staining results were consistent with those obtained from the plate counting method. In PBS, PBS+NIR, and BP groups, the bacterial cells showed strong green fluorescence but no red fluorescence, suggesting that *E. coli* and *S. aureus* were all alive. After treatment of BP-QCS and BP with NIR, the intensity of green fluorescence decreased, whereas that of red fluorescence increased, indicating that many bacteria died. The live/dead cell ratio of BP with NIR was lower than that of BP-QCS without NIR irradiation. The BP-QCS+NIR group showed the lowest live/dead cell ratio, revealing the highest bactericidal efficiency.

The morphology and the membrane integrity of *E. coli* and *S. aureus* cells after treatment with BP-QCS and BP-QCS+NIR exposure were examined by FE-SEM (Figure 7). *E. coli* and *S. aureus* cultured in the presence of BP-QCS slightly shrunk and deformed with some BP-QCS attached into their surface, suggesting that BP-QCS has a certain antibacterial effect even without NIR irradiation. The morphology of *E. coli* and *S. aureus* cells was completely destroyed in the BP-QCS+NIR group, and most of the cells aggregated together with BP-QCS attached.

Drug Resistance Study. To investigate whether BP-QCS will induce drug resistance, doxycycline as a widely used antibiotic in clinics was taken for comparison. MRSA bacteria were treated with BP-QCS or doxycycline at sublethal
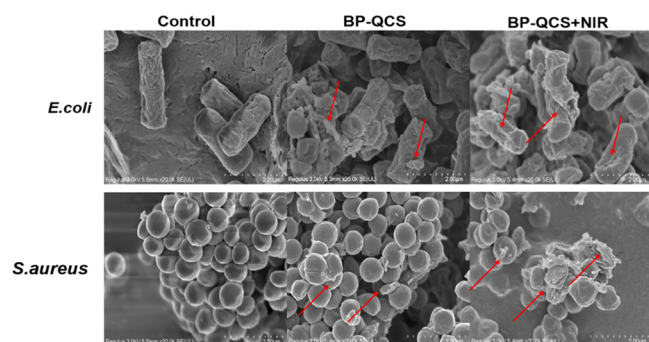
Figure 7. FE-SEM images of *E. coli* (top panel) and *S. aureus* (bottom panel) treated with BP-QCS and BP-QCS+NIR.

concentration for 10 passages, and the antibacterial activity was compared at different passages. Multiple exposures of MRSA bacteria to doxycycline gradually result in the evolution of drug resistance (Figure 8b). Comparatively, BP-QCS still keep high
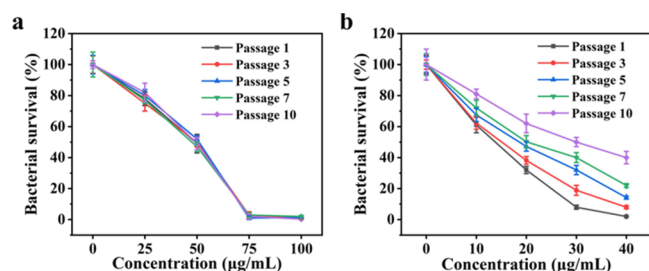

Figure 8. Development of drug resistance. Antibacterial profiles of (a) BP-QCS and (b) doxycycline against MRSA bacteria after multiple treatments at sublethal concentrations.

antibacterial activity even after 10 passages (Figure 8a). Therefore, BP-QCS has little risk of drug resistance, making it a promising antibacterial platform.

In Vitro Biocompatibility. In therapy, cytotoxicity is a key factor that affects application of a new drug or material. Cytotoxicity of BP-QCS was assessed using MTT measurement (Figure 9a). The MTT assay protocol is based on the viable cell-activated conversion of the water-soluble 3-(4,5-dimethylthiazol-2-yl)-2,5-diphenyltetrazolium bromide compound to a purple insoluble formazan product, whose absorbance at OD 590 nm is proportional to the number of viable cells. When the concentration of BP-QCS was as high as 125 μg/mL, 86% of the cells was still alive, revealing that the as-prepared BP-QCS had negligible cytotoxicity because a

survival rate greater than 80% can be considered as nontoxic to cells.[56,57]

We also studied biocompatibility of BP-QCS by a hemolytic test as the hemolytic property is another key factor (Figure 9b). The hemolysis percentage of red blood cells was less than 5% when they were cultured with 125 μg/mL BP-QCS, indicating a quite good biocompatibility of BP-QCS.

In Vivo Antibacterial Activity. We designed an infection model by injecting *S. aureus* subcutaneously into the back of mice in order to assess the in vivo antibacterial capacity of BP-QCS. All infected mice with subcutaneous abscesses were divided into six groups in the same way as above. Figure 10a shows the schematic arrangement of the experimental device. We studied the in vivo photothermal effect of BP-QCS through thermal imaging (Figure 10b). After irradiation with the NIR laser for 10 min, the temperatures of the infected sites in BP and BP-QCS groups increased from 37 to 52 °C and 37.2 to 51.9 °C, respectively, whereas the temperature of the infected site in the PBS group increased only by 2 °C. The results indicate that the as-prepared BP-QCS also has high photothermal efficiency not only in vitro but also in vivo.

We monitored the infected sites of the mouse skin for 8 days after single treatment (Figure 10c,d), to evaluate the in vivo photothermal antibacterial ability of BP-QCS. In the BP-QCS plus NIR irradiation group, no obvious wound or ulcer was observed at the infected site 8 days after treatment, whereas in other groups, the wounds shrunk but were still obvious. Thus, BP-QCS plus NIR irradiation has the best in vivo antibacterial ability.

Mice were sacrificed on the 8th day for bacterial quantification and H&E staining. As shown in Figure 10e, for the BP-QCS plus NIR group, only few individual colonies formed on the plate, whereas the remaining groups had much more colonies. The PBS group was used as a control to calculate the relative bacterial survival rate (Figure 10f). Both NIR and BP alone had a negligible antibacterial effect, as their bacterial survival rates were greater than 90% after the treatment; however, BP-QCS alone and BP plus NIR had a moderate antibacterial ability, showing bacterial survival rates between 50 and 70%. In contrast, BP-QCS plus NIR, the most effective method tested here, killed 98% of the bacteria, which is in agreement with the results of in vitro experiments.

The skin infection sites were further analyzed by H&E staining (Figure 11a). In the BP-QCS plus NIR group, the intact skin tissue was clearly observed. However, for other groups, obvious inflammation and tissue damage can be seen (the red arrows represent the location of inflammatory cell
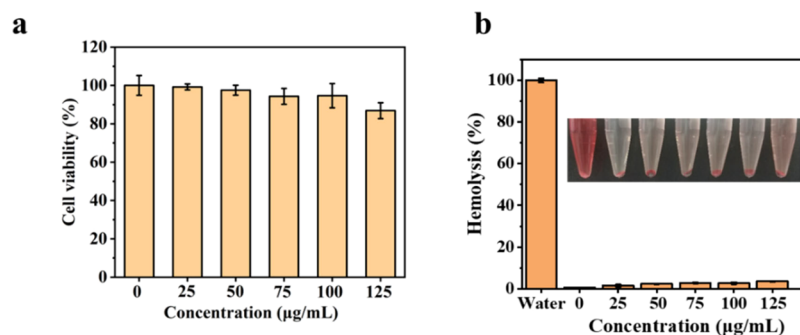

Figure 9. Biocompatibility analysis. (a) Cell viability of 3T3 after being cultured with different concentrations of BP-QCS. (b) Hemolytic assay of red blood cells at various concentrations of BP-QCS. The inset shows the corresponding photographs of the different conditions.
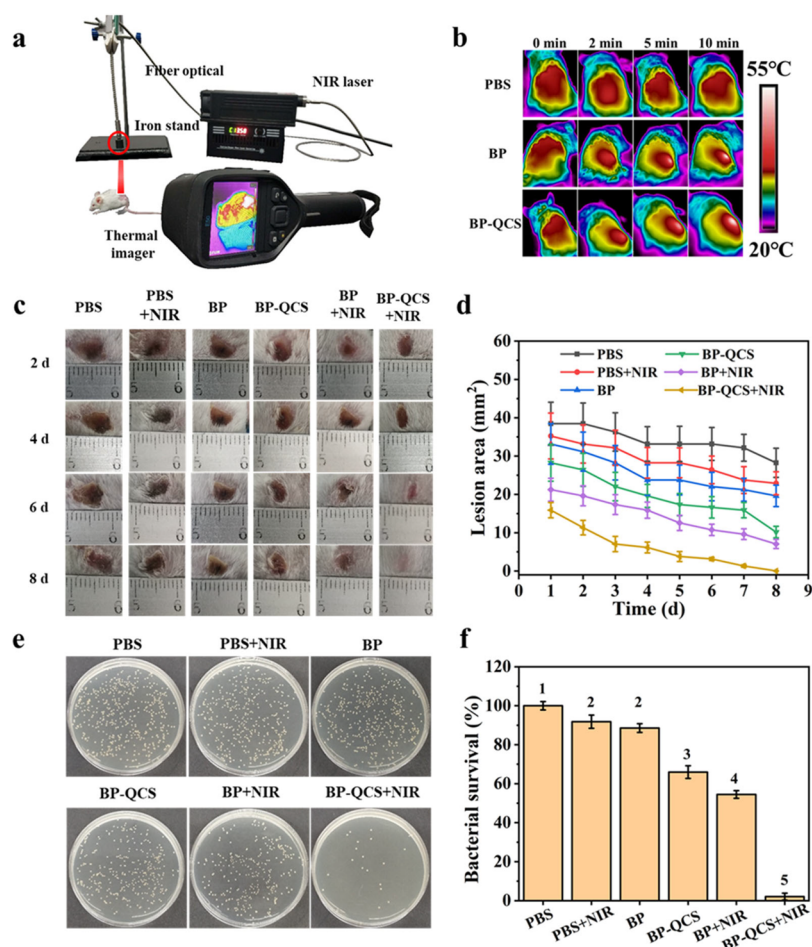
Figure 10. In vivo antibacterial activity. (a) Schematic of the experimental device. (b) Photothermal imaging of mice treated with PBS, BP nanosheets, and BP-QCS under 808 nm laser irradiation (1 W/cm^2) for 10 min. (c) Photographs of the infectious sites at 2, 4, 6, and 8 days after different treatments. (d) Lesion area of the wounds at different time points. (e) Photographs of bacterial colonies obtained from infected tissues of mice. (f) Relative bacterial survival rates after various treatments. 1−5 indicate that the groups marked with different numbers have significant differences ($p < 0.05$).
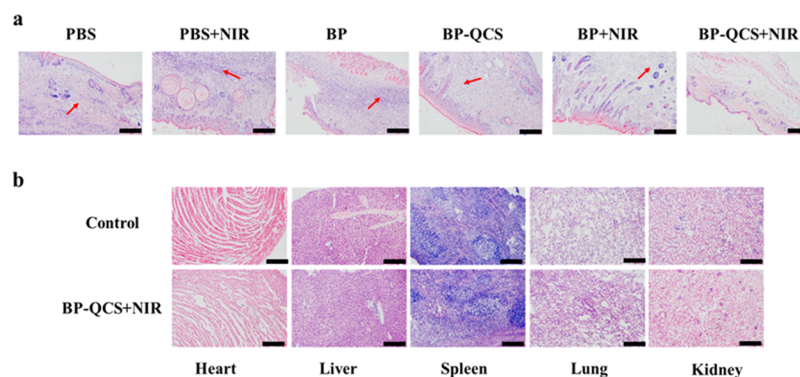

Figure 11. H&E staining results of (a) skin lesions and (b) main organs (the heart, liver, spleen, lungs, and kidney). The scale bar is 200 μm.

infiltration). In addition, no obvious histological damage of main organs was found in mice of the BP-QCS plus NIR group when compared with the control group according to the H&E staining results (Figure 11b).

■ EXPERIMENTAL SECTION

Materials. The bulk BP crystals were obtained from XFNANO (Nanjing, China). CS (degree of deacetylation, 90%) and glycidyltrimethylammonium chloride (GTA) were purchased from

Shanghai Macklin Biochemical Co., Ltd. (Shanghai, China). A yeast extract, tryptone, and agar powder were supplied by Solarbio (Beijing, China). Dimethyl sulfoxide (DMSO), AgNO$_3$, NaCl, KCl, Na$_2$HPO$_4$, and KH$_2$PO$_4$ were purchased from Sinopharm Chemical Reagent (Beijing, China). A Calcein-AM/PI Double Stain Kit was obtained from Gibco (California, USA). Ultrapure water was provided by Wahaha Group Co. (Hangzhou, China).

E. coli (ATCC 25922), *S. aureus* (ATCC 43300), and methicillin-resistant *S. aureus* (MRSA, ATCC43300) were provided by the School of Food Science and Technology, Jiangnan University (Wuxi,

China) and the School of Radiation Medicine and Protection, Soochow University (Soochow, China). 3T3 cells, an embryonic fibroblast cell line commonly used for MTT analysis, were purchased from Fenghui Biotechnology Co., Ltd. (Hunan, China).

Synthesis. We synthesized BP nanosheets by ultrasonication-assisted aqueous-phase exfoliation. In brief, 25 mg of bulk BP was wet ground in a mortar, 25 mL of water was then added, and the dispersion was sonicated for 10 h in an ice bath using a Scientz-IID ultrasonic homogenizer (Ningbo, China). The power was 300 W, and a sonicating microtip of 8 mm diameter worked for 4 s with an idle interval of 4 s. Afterward, the mixture was centrifuged at 4000 rpm for 10 min to remove large nonexfoliated BP, and then, the supernatant was further centrifuged at 12,000 rpm for 20 min to collect BP nanosheets. The precipitate was freeze-dried and stored in a nitrogen-filled dryer for further experiments. To synthesize QCS, 1 g of CS and 5 g of GTA were added to 30 mL of water and then stirred at 80 °C for 12 h. The mixture was centrifuged at 4000 rpm for 10 min to discard unreacted CS. The supernatant was dialyzed in a dialysis bag (12,000 Da) for 2 days. We estimated the concentration of QCS in the dialysate via titration with 0.1 mol/L $AgNO_3$ solution until there was no white precipitate. Finally, QCS was obtained by freeze-drying. To fabricate BP-QCS, 2 mg of BP nanosheets and 5 mg of QCS were added to 5 mL of water, sonicated for 30 min, and then stirred for 3 h at room temperature. The sample was centrifuged at 12,000 rpm for 20 min, washed twice with water, and obtained by freeze-drying.

Characterization. The transmission electron microscopy (TEM) and atomic force microscopy (AFM) images of BP nanosheets were acquired on a JEM-2100 transmission electron microscope (JEOL, Japan) and a Dimension Icon atomic force microscope (Bruker, USA), respectively. The scanning transmission electron microscopy (STEM) image and elemental mapping were examined using a TALOS F200 field emission high-resolution transmission electron microscope (FEI, USA). FTIR spectra of CS and QCS were obtained using an IS10 Fourier transform infrared spectrometer (Nicolet, USA). The conductivities of the samples were measured using an S700-B conductivity meter (METTLER TOLEDO, Switzerland). The zeta potentials were measured and dynamic light scattering (DLS) was performed on a ZEN3700 nanolaser particle size analyzer (Malvern, UK). The UV−NIR absorption spectra were acquired on a UV-3600-PLUS UV−Vis−NIR spectrophotometer (Shimadzu, Japan).

Stability Studies. The solubility of BP-QCS in PBS, including NaCl, KCl, Na_2HPO_4, and KH_2PO_4, was first studied. BP-QCS (100 μg/mL) was thoroughly dispersed into PBS using ultrasound and kept at room temperature for 12 h. The state of the suspensions was then observed. The stability of the BP-QCS suspensions was investigated by measuring their absorption daily for 7 days. For comparison, BP (100 μg/mL) was also processed as above.

Photothermal Effect. BP-QCS (1 mL, 75 μg/mL) and BP (1 mL, 75 μg/mL) in PBS were irradiated with an 808 nm semiconductor laser (Viasho Technology, Beijing, China). PBS served as a blank control. The power density was 1 W/cm², and the irradiation time was 10 min. The temperature was recorded using an infrared thermal imager (FLIR, USA). The photothermal effects of BP-QCS at different concentrations (25, 50, 75, 100, and 125 μg/mL) were measured following a similar procedure. To investigate the photothermal stability of BP-QCS, 1 mL of BP-QCS suspensions (75 μg/mL) in PBS was repeatedly irradiated five times. Photothermal conversion efficiency (η) of BP-QCS was then calculated according to the methods reported previously.[14,57,58]

In Vitro Antibacterial Experiments. *E. coli* and *S. aureus* were chosen as Gram-negative and Gram-positive model microbes, and methicillin-resistant *S. aureus* was chosen as a drug-resistant model microbe to evaluate the antibacterial efficiency. They were incubated in a lysogenic broth (LB) medium and allowed to grow at 37 °C and 180 rpm. The bacterial suspensions were centrifuged at 5000 rpm for 3 min, and the precipitate was washed twice with PBS to remove the culture medium. Finally, bacteria were resuspended in PBS, and the concentration of the two bacterial suspensions was adjusted to 10^8 CFU/mL. The bacterial suspension (100 μL, 10^8 CFU/mL) was

mixed with the materials, and the volume was adjusted to 1 mL with PBS.

First, the experimental conditions were optimized. When the laser power is constant (1 W/cm²), the antibacterial efficiency is affected by the irradiation time and the concentration of BP-QCS. They need to be optimized to determine the shortest irradiation time and the lowest concentration that can effectively kill bacteria. The irradiation time (2.5, 5, 7.5, 10, and 12.5 min, [BP-QCS] = 75 μg/mL) and the concentrations of the BP-QCS (0, 25, 50, 75, 100, and 125 μg/mL, irradiation time = 10 min) were screened to determine the optimum experimental conditions. The bacterial survival rate was obtained to determine the optimum experimental conditions.

Then, the next experiment was carried out under optimal conditions. The experiment was divided into six groups: (1) PBS, (2) PBS+NIR, (3) BP, (4) BP-QCS, (5) BP+NIR, and (6) BP-QCS +NIR. For groups (3) to (6), the concentration of BP or BP-QCS was 75 μg/mL. All groups were incubated for 1 h at 37 °C. For groups (2), (5), and (6), samples were irradiated with an 808 nm laser (1 W/ cm²) for 10 min. Then, the suspensions were diluted by 10^4 times, and 100 μL of each was added to the LB plate. The number of colonies was recorded after incubation at 37 °C for 12 h.

LIVE/DEAD Fluorescence Staining Assay. After different treatments, the bacterial suspensions were centrifuged at 5000 rpm for 3 min and then stained with the Calcein-AM/PI Double Stain Kit according to the manufacturer's instructions. Then, 10 μL of the bacterial suspension was placed on a glass slide and imaged using a laser scanning confocal microscope (Olympus, USA). Live bacteria were labeled by Calcein-AM and showed green fluorescence, whereas dead bacteria were stained by PI and displayed red fluorescence.

Biocompatibility Assay. Cytotoxicity of the material was detected by succinate dehydrogenase activity assay (MTT method). 3T3 cells were seeded on a 96-well plate, and the density was 1×10^4 cells per well. After incubation (37 °C, 5% CO_2) for 16 h, the upper medium was removed, and 100 μL of BP-QCS suspensions with different concentrations (0, 25, 50, 75, 100, and 125 μg/mL) was added. After culturing overnight, the medium was replaced with 100 μL of 3-(4,5-dimethylthiazol-2-yl)-2,5-diphenyltetrazolium bromide (the MTT solution, 0.5 mg/mL) and further incubated for 4 h. Then, the upper medium was removed, and 150 μL of DMSO was added to each well. A Synergy H1 microplate reader (BioTek, USA) was used to obtain the absorbance of each well at 570 nm. For hemolytic analysis, whole blood of mice was centrifuged and washed several times with PBS until the supernatant did not show red. Then, 500 μL of the 4% red blood cell suspension was added into 500 μL of BP suspensions with different concentrations (0, 50, 100, 150, 200, and 250 μg/mL) and incubated at 37 °C for 1 h. After centrifugation at 5000 rpm for 5 min, the absorbance of the supernatant was measured using a spectrometer at 540 nm. The hemolysis rate was calculated according to the following equation

$$\text{Hemolysis (\%)} = (I/I_0) \times 100\%$$

where I is the absorbance value of the supernatant and I_0 is the absorbance value when the red blood cells are completely hemolyzed in water.

Drug Resistance Study. To study drug resistance, MRSA bacteria were incubated with doxycycline (2.5 μg/mL) for 10 passages. The antibacterial activity of doxycycline (0, 10, 20, 30, and 40 μg/mL) against each passage of MRSA bacteria (10^7 CFU/mL) was measured by agar plate assay after 1 h incubation.

For BP-QCS, MRSA bacteria were initially incubated with BP-QCS (50 μg/mL) for 12 h. The antibacterial activity of BP-QCS (0, 25, 50, 75, and 100 μg/mL) against MRSA bacteria (10^7 CFU/mL) was measured by agar plate assay after 1 h incubation and 10 min irradiation using an 808 nm laser at 1 W/cm². This is the first passage and the first cycle. Then, 10 μL of bacterial solution was removed from the 50 μg/mL BP-QCS group after irradiation, cultured in a medium with 50 μg/mL BP-QCS for 12 h, and tested for antibacterial activity of these bacteria against BP-QCS (0, 25, 50, 75, and 100 μg/ mL). The process was also repeated for 10 passages.

In Vivo Antibacterial Experiment. BALB/c mice (4 weeks old, 16−18 g) were purchased from SLAC Laboratory Animal Co., Ltd. (Shanghai, China). All animal experiments were carried out according to the regulations of the Animal Experiment Center of Jiangnan University. *S. aureus*-infected mice were used as model animals to further evaluate the antibacterial properties of the material. The experimental mice were divided into six groups, three mice each, and the treatment of each group was (1) PBS, (2) PBS+NIR, (3) BP, (4) BP-QCS, (5) BP+NIR, and (6) BP-QCS+NIR. Before the experiment, the *S. aureus* suspension (10^8 CFU/mL, 100 μL) was injected into the back of the mice. The experimental mice with subcutaneous abscesses were divided 24 h after injection. Then, 100 μL of different materials (BP and BP-QCS were both 75 μg/mL) was subcutaneously injected into the abscess sites of the mice in each corresponding group. For groups (2), (5), and (6), 5 min after injection, the abscess sites were irradiated with an 808 nm laser for 10 min, and the power was 1 W/cm^2. The remaining three groups were treated in the same way except NIR irradiation. The abscess sites of each group were monitored and photographed daily for 8 days. All mice were euthanized on the eighth day. The infected sites were excised and divided into two parts. One part was homogenized for clone formation analysis to calculate the relative survival rate of the bacteria, and the other part was fixed in 4% paraformaldehyde for hematoxylin and eosin (H&E) staining. In addition, the main organs (the heart, liver, spleen, lungs, and kidney) of the sixth group and normal mice were also taken for H&E staining.

CONCLUSIONS

We developed a highly biocompatible synergetic antibacterial method based on BP nanosheets and QCS. We increased the stability of BP nanosheets significantly by electrostatically adsorbing QCS onto BP without affecting the photothermal efficiency of BP nanosheets. The photothermal properties of BP nanosheets and the bacteriostatic performance of QCS displayed a synergetic effect on disinfection. Both in vitro and in vivo studies indicated an excellent antibacterial ability and relatively low toxicity of BP-QCS plus irradiation of NIR light. Thus, BP-QCS has showed great potential in future clinical applications of photothermal therapy, especially in photothermal disinfection.

ASSOCIATED CONTENT

Supporting Information

The Supporting Information is available free of charge at https://pubs.acs.org/doi/10.1021/acsabm.1c00054.

Additional figures, including absorption spectra of BP and bulk BP, photograph of CS and QCS dispersed in water, conductometric titration of QCS by AgNO$_3$, bacterial viability of *E. coli* and *S. aureus* after treatments with different irradiation times and concentrations of BP-QCS, bacterial viability of *E. coli* and *S. aureus* after treatments with different concentrations of CS and QCS, and cell viability of 3T3 after being cultured with different concentrations of CS and QCS (PDF)

AUTHOR INFORMATION

Corresponding Author

Yi Zhang − *State Key Laboratory of Food Science and Technology, Collaborative Innovation Center of Food Safety and Quality Control in Jiangsu Province, and Institute of Analytical Food Safety, School of Food Science and Technology, Jiangnan University, Wuxi 214122, China;* orcid.org/0000-0002-2500-680X; Email: zhangyijnu@jiangnan.edu.cn

Authors

Xu-Fang Qu − *Institute of Analytical Food Safety, School of Food Science and Technology, Jiangnan University, Wuxi 214122, China*

Cheng-Long Zhu − *Institute of Analytical Food Safety, School of Food Science and Technology, Jiangnan University, Wuxi 214122, China*

Han-Jie Yang − *Institute of Analytical Food Safety, School of Food Science and Technology, Jiangnan University, Wuxi 214122, China*

Chen-Hui Lu − *Institute of Analytical Food Safety, School of Food Science and Technology, Jiangnan University, Wuxi 214122, China*

Wen-Long Wang − *Institute of Analytical Food Safety, School of Food Science and Technology, Jiangnan University, Wuxi 214122, China*

Yuehong Pang − *State Key Laboratory of Food Science and Technology, Jiangnan University, Wuxi 214122, China;* orcid.org/0000-0002-8050-7375

Cheng Yang − *Institute of Analytical Food Safety, School of Food Science and Technology, Jiangnan University, Wuxi 214122, China*

Li-Jian Chen − *State Key Laboratory of Food Science and Technology, Collaborative Innovation Center of Food Safety and Quality Control in Jiangsu Province, and Institute of Analytical Food Safety, School of Food Science and Technology, Jiangnan University, Wuxi 214122, China;* orcid.org/0000-0001-8671-8766

Xing-Fang Li − *Division of Analytical and Environmental Toxicology, Department of Laboratory Medicine and Pathology, Faculty of Medicine and Dentistry, University of Alberta, Edmonton, Alberta T6G 2G3, Canada;* orcid.org/0000-0003-1844-7700

Complete contact information is available at:
https://pubs.acs.org/10.1021/acsabm.1c00054

Author Contributions

The manuscript was written through contributions of all authors. All authors have given approval to the final version of the manuscript.

Notes

The authors declare no competing financial interest.

ACKNOWLEDGMENTS

ABBREVIATIONS

BP, black phosphorus; CS, chitosan; QCS, quaternized chitosan; ROS, reactive oxygen species; GTA, glycidyltrimethylammonium chloride

■ REFERENCES

(1) Allegranzi, B.; Bagheri Nejad, S.; Combescure, C.; Graafmans, W.; Attar, H.; Donaldson, L.; Pittet, D. Burden of Endemic Health-Care-Associated Infection in Developing Countries: Systematic Review and Meta-Analysis. *Lancet* **2011**, *377*, 228−241.

(2) Fears, R.; van der Meer, J. W.; ter Meulen, V. The Changing Burden of Infectious Disease in Europe. *Sci. Transl. Med.* **2011**, *90*, 103cm30.

(3) Teng, C. P.; Zhou, T.; Ye, E.; Liu, S.; Koh, L. D.; Low, M.; Loh, X. J.; Win, K. Y.; Zhang, L.; Han, M. Y. Effective Targeted Photothermal Ablation of Multidrug Resistant Bacteria and Their Biofilms with NIR-Absorbing Gold Nanocrosses. *Adv. Healthcare Mater.* **2016**, *5*, 2122−2130.

(4) Zhang, X.; Wu, J.; Williams, G. R.; Niu, S.; Qian, Q.; Zhu, L.-M. Functionalized MoS_2-Nanosheets for Targeted Drug Delivery and Chemo-Photothermal Therapy. *Colloids Surf., B* **2019**, *173*, 101−108.

(5) Zhu, H.; Ni, N.; Govindarajan, S.; Ding, X.; Leong, D. T. Phototherapy with Layered Materials Derived Quantum Dots. *Nanoscale* **2020**, *12*, 43−57.

(6) Zhao, J.; Huang, S.; Ravisankar, P.; Zhu, H. Two-Dimensional Nanomaterials for Photoinduced Antibacterial Applications. *ACS Appl. Bio Mater.* **2020**, *3*, 8188−8210.

(7) Yang, G.; Liu, Z.; Li, Y.; Hou, Y.; Fei, X.; Su, C.; Wang, S.; Zhuang, Z.; Guo, Z. Facile Synthesis of Black Phosphorus−Au Nanocomposites for Enhanced Photothermal Cancer Therapy and Surface-Enhanced Raman Scattering Analysis. *Biomater. Sci.* **2017**, *5*, 2048−2055.

(8) Ou, W.; Byeon, J. H.; Thapa, R. K.; Ku, S. K.; Yong, C. S.; Kim, J. O. Plug-and-Play Nanorization of Coarse Black Phosphorus for Targeted Chemo-Photoimmunotherapy of Colorectal Cancer. *ACS Nano* **2018**, *12*, 10061−10074.

(9) Li, M.; Li, L. Q.; Su, K.; Liu, X. M.; Zhang, T. J.; Liang, Y. Q.; Jing, D. D.; Yang, X. J.; Zheng, D.; Cui, Z. D.; Li, Z. Y.; Zhu, S. L.; Yeung, K. W. K.; Zheng, Y. F.; Wang, X. B.; Wu, S. L. Highly Effective and Noninvasive Near-Infrared Eradication of a Staphylococcus aureus Biofilm on Implants by a Photoresponsive Coating within 20 Min. *Adv. Sci.* **2019**, *6*, 1900599.

(10) Chen, W.; Ouyang, J.; Liu, H.; Chen, M.; Zeng, K.; Sheng, J.; Liu, Z.; Han, Y.; Wang, L.; Li, J.; Deng, L.; Liu, Y. N.; Guo, S. Black Phosphorus Nanosheet-Based Drug Delivery System for Synergistic Photodynamic/Photothermal/Chemotherapy of Cancer. *Adv. Mater.* **2017**, *29*, 1603864−1603870.

(11) Carling, C.-J.; Nourmohammadian, F.; Boyer, J.-C.; Branda, N. R. Remote-Control Photorelease of Caged Compounds Using Near-Infrared Light and Upconverting Nanoparticles. *Angew. Chem., Int. Ed.* **2010**, *49*, 3782−3785.

(12) Ardakani, T. S.; Meidanchi, A.; Shokri, A.; Shakeri-Zadeh, A. Fe_3O_4@Au/Reduced Graphene Oxide Nanostructures: Combinatorial Effects of Radiotherapy and Photothermal Therapy on Oral Squamous Carcinoma KB Cell Line. *Ceram. Int.* **2020**, *46*, 28676−28685.

(13) Xie, X.; Mao, C.; Liu, X.; Tan, L.; Cui, Z.; Yang, X.; Zhu, S.; Li, Z.; Yuan, X.; Zheng, Y.; Yeung, K. W. K.; Chu, P. K.; Wu, S. Tuning the Bandgap of Photo-Sensitive Polydopamine/Ag_3PO_4/Graphene Oxide Coating for Rapid, Noninvasive Disinfection of Implants. *ACS Central. Sci.* **2018**, *4*, 724−738.

(14) Zhu, H.; Lai, Z.; Fang, Y.; Zhen, X.; Tan, C.; Qi, X.; Ding, D.; Chen, P.; Zhang, H.; Pu, K. Ternary Chalcogenide Nanosheets with Ultrahigh Photothermal Conversion Efficiency for Photoacoustic Theranostics. *Small* **2017**, *13*, 1604139.

(15) Zhu, M.; Liu, X.; Tan, L.; Cui, Z.; Liang, Y.; Li, Z.; Yeung, K. W. K.; Wu, S. Photo-responsive chitosan/Ag/MoS_2 for rapid bacteria-killing. *J. Hazard. Mater.* **2020**, *383*, 121122.

(16) Chang, M.; Hou, Z.; Wang, M.; Wang, M.; Dang, P.; Liu, J.; Shu, M.; Ding, B.; Al Kheraif, A. A.; Li, C.; Lin, J. Cu_2MoS_4/Au Heterostructures with Enhanced Catalase-Like Activity and Photoconversion Efficiency for Primary/Metastatic Tumors Eradication by Phototherapy-Induced Immunotherapy. *Small* **2020**, *16*, 1907146.

(17) Han, D.; Han, Y.; Li, J.; Liu, X.; Yeung, K. W. K.; Zheng, Y.; Cui, Z.; Yang, X.; Liang, Y.; Li, Z.; Zhu, S.; Yuan, X.; Feng, X.; Yang, C.; Wu, S. Enhanced photocatalytic activity and photothermal effects of Cu-doped metal-organic frameworks for rapid treatment of bacteria-infected wounds. *Appl. Catal. B-Environ.* **2020**, *261*, 118248.

(18) Cai, X.; Gao, W.; Zhang, L.; Ma, M.; Liu, T.; Du, W.; Zheng, Y.; Chen, H.; Shi, J. Enabling Prussian Blue with Tunable Localized Surface Plasmon Resonances: Simultaneously Enhanced Dual-Mode Imaging and Tumor Photothermal Therapy. *ACS Nano* **2016**, *10*, 11115−11126.

(19) Fu, H.; Li, Z.; Xie, H.; Sun, Z.; Wang, B.; Huang, H.; Han, G.; Wang, H.; Chu, P. K.; Yu, X. F. Different-Sized Black Phosphorus Nanosheets with Good Cytocompatibility and High Photothermal Performance. *RSC Adv.* **2017**, *7*, 14618−14624.

(20) Naskar, A.; Kim, K. S. Black Phosphorus Nanomaterials as Multi-Potent and Emerging Platforms against Bacterial Infections. *Microb. Pathogenesis.* **2019**, *137*, 103800.

(21) Li, S.; Zhang, Y.; Wen, W.; Sheng, W.; Wang, J.; Wang, S.; Wang, J. A High-Sensitivity Thermal Analysis Immunochromatographic Sensor Based on Au Nanoparticle-Enhanced Two-Dimensional Black Phosphorus Photothermal-Sensing Materials. *Biosens. Bioelectron.* **2019**, *133*, 223−229.

(22) Chen, W.; Ouyang, J.; Yi, X.; Xu, Y.; Niu, C.; Zhang, W.; Wang, L.; Sheng, J.; Deng, L.; Liu, Y.-N.; Guo, S. Black Phosphorus Nanosheets as a Neuroprotective Nanomedicine for Neurodegenerative Disorder Therapy. *Adv. Mater.* **2018**, *30*, 1703458.

(23) Qiu, M.; Wang, D.; Liang, W.; Liu, L.; Zhang, Y.; Chen, X.; Sang, D. K.; Xing, C.; Li, Z.; Dong, B.; Xing, F.; Fan, D.; Bao, S.; Zhang, H.; Cao, Y. Novel Concept of the Smart NIR-Light−Controlled Drug Release of Black Phosphorus Nanostructure for Cancer Therapy. *Proc. Natl. Acad. Sci. U. S. A.* **2018**, *115*, 501−506.

(24) Wang, Y.; Hu, X.; Zhang, L.; Zhu, C.; Wang, J.; Li, Y.; Wang, Y.; Wang, C.; Zhang, Y.; Yuan, Q. Bioinspired Extracellular Vesicles Embedded with Black Phosphorus for Molecular Recognition-guided Biomineralization. *Nat. Commun.* **2019**, *10*, 2829.

(25) Li, Y.; Liu, Z.; Hou, Y.; Yang, G.; Fei, X.; Zhao, H.; Guo, X.; Su, C.; Wang, Z.; Zhong, H.; Zhuang, Z.; Guo, Z. Multifunctional Nanoplatform Based on Black Phosphorus Quantum Dots for Bioimaging and Photodynamic/Photothermal Synergistic Cancer Therapy. *ACS Appl. Mater. Interfaces* **2017**, *9*, 25098−25106.

(26) Shao, J.; Xie, H.; Huang, H.; Li, Z.; Sun, Z.; Xu, Y.; Xiao, Q.; Yu, X. F.; Zhao, Y.; Zhang, H.; Wang, H.; Chu, P. K. Biodegradable Black Phosphorus-Based Nanospheres for in vivo Photothermal Cancer Therapy. *Nat. Commun.* **2016**, *7*, 12967−12979.

(27) Shao, J.; Ruan, C.; Xie, H.; Li, Z.; Wang, H.; Chu, P. K.; Yu, X. F. Black-Phosphorus-Incorporated Hydrogel as a Sprayable and Biodegradable Photothermal Platform for Postsurgical Treatment of Cancer. *Adv. Sci.* **2018**, *5*, 1700848−1700858.

(28) Yang, Y.; Zeng, B.; Guo, J.; Li, Y.; Yang, Y.; Yuan, Q. Two-Dimensional Device with Light-Controlled Capability for Treatment of Cancer-Relevant Infection Diseases. *Anal. Chem.* **2020**, *92*, 10162−10168.

(29) Ouyang, J.; Liu, R. Y.; Chen, W.; Liu, Z.; Xu, Q.; Zeng, K.; Deng, L.; Shen, L.; Liu, Y. N. A Black Phosphorus Based Synergistic Antibacterial Platform Against Drug Resistant Bacteria. *J. Mater. Chem. B* **2018**, *6*, 6302−6310.

(30) Guo, T.; Zhuang, S.; Qiu, H.; Guo, Y.; Wang, L.; Jin, G.; Lin, W.; Huang, G.; Yang, H. Black Phosphorus Nanosheets for Killing Bacteria through Nanoknife Effect. *Part. Part. Syst. Charact.* **2020**, *37*, 2000169.

(31) Liu, W.; Zhang, Y.; Zhang, Y.; Dong, A. Black Phosphorus Nanosheets Counteract Bacteria without Causing Antibiotic Resistance. *Chem-Eur. J.* **2020**, *26*, 2478−2485.

(32) Liang, M.; Zhang, M.; Yu, S.; Wu, Q.; Ma, K.; Chen, Y.; Liu, X.; Li, C.; Wang, F. Silver-Laden Black Phosphorus Nanosheets for an Efficient in Vivo Antimicrobial Application. *Small* **2020**, *16*, 1905938.

(33) Zhang, D.; Liu, H. M.; Shu, X.; Feng, J.; Yang, P.; Dong, P.; Xie, X.; Shi, Q. Nanocopper-Loaded Black Phosphorus Nanocomposites

for Efficient Synergistic Antibacterial Application. *J. Hazard. Mater.* **2020**, *393*, 122317.

(34) He, D.; Zhang, Z.; Xing, Y.; Zhou, Y.; Yang, H.; Liu, H.; Qu, J.; Yuan, X.; Guan, J.; Zhang, Y. Black Phosphorus/Graphitic Carbon Nitride: a Metal-Free Photocatalyst for "Green" Photocatalytic Bacterial Inactivation under Visible Light. *Chem. Eng. J.* **2019**, *384*, 123258.

(35) Aksoy, İ.; Küçükkeçeci, H.; Sevgi, F.; Metin, Ö.; Patir, I. H. Photothermal Antibacterial and Antibiofilm Activity of Black Phosphorus/Gold Nanocomposites Against Pathogenic Bacteria. *Acs Appl. Mater. Inter.* **2020**, *12*, 26822−26831.

(36) Zhang, C.; Wang, Y.; Ma, J.; Zhang, Q.; Wang, F.; Liu, X.; Xia, T. Black Phosphorus for Fighting Antibiotic-Resistant Bacteria: What Is Known and What Is Missing. *Sci. Total Environ.* **2020**, *721*, 137740.

(37) Li, Z.; Wu, L.; Wang, H.; Zhou, W.; Liu, H.; Cui, H.; Li, P.; Chu, P. K.; Yu, X.-F. Synergistic Antibacterial Activity of Black Phosphorus Nanosheets Modified with Titanium Aminobenzenesulfanato Complexes. *Acs Appl. Nano Mater.* **2019**, *2*, 1202−1209.

(38) Tan, L.; Li, J.; Liu, X.; Cui, Z.; Yang, X.; Yeung, K. W. K.; Pan, H.; Zheng, Y.; Wang, X.; Wu, S. In Situ Disinfection through Photoinspired Radical Oxygen Species Storage and Thermal-Triggered Release from Black Phosphorous with Strengthened Chemical Stability. *Small* **2018**, *14*, 1703197−1703207.

(39) Zhang, L.; Wang, Y.; Wang, J.; Wang, Y.; Chen, A.; Wang, C.; Mo, W.; Li, Y.; Yuan, Q.; Zhang, Y. Photon-Responsive Antibacterial Nanoplatform for Synergistic Photothermal-/Pharmaco-Therapy of Skin Infection. *Acs Appl. Mater. Inter.* **2019**, *11*, 300−310.

(40) Sudheesh Kumar, P. T.; Lakshmanan, V. K.; Anilkumar, T. V.; Ramya, C.; Reshmi, P.; Unnikrishnan, A. G.; Nair, S. V.; Jayakumar, R. Flexible and Microporous Chitosan Hydrogel/Nano ZnO Composite Bandages for Wound Dressing: in Vitro and in Vivo Evaluation. *Acs Appl. Mater. Inter.* **2012**, *4*, 2618−2629.

(41) Kim, I. Y.; Seo, S. J.; Moon, H. S.; Yoo, M. K.; Park, I. Y.; Kim, B. C.; Cho, C. S. Chitosan and Its Derivatives for Tissue Engineering Applications. *Biotechnol. Adv.* **2008**, *26*, 1−21.

(42) Dodane, V.; Vilivalam, V. D. Pharmaceutical Applications of Chitosan. *Pharm. Sci. Technol. To.* **1998**, *1*, 246−253.

(43) Mawad, A.; Helmy, Y. A.; Shalkami, A.-G.; Kathayat, D.; Rajashekara, G. E. coli Nissle Microencapsulation in Alginate-Chitosan Nanoparticles and Its Effect on Campylobacter Jejuni in Vitro. *Appl. Microbiol. Biot.* **2018**, *102*, 10675−10690.

(44) Mao, C.; Xiang, Y.; Liu, X.; Cui, Z.; Yang, X.; Li, Z.; Zhu, S.; Zheng, Y.; Yeung, K. W. K.; Wu, S. Repeatable Photodynamic Therapy with Triggered Signaling Pathways of Fibroblast Cell Proliferation and Differentiation to Promote Bacteria-Accompanied Wound Healing. *ACS Nano* **2018**, *12*, 1747−1759.

(45) Li, D.; Zhao, Q.; Zhang, S.; Wu, F.; Yu, X.; Xiong, Z.; Ma, W.; Wang, D.; Zhang, X.; Xing, B. Filtration-Based Water Treatment System Embedded with Black Phosphorus for NIR-Triggered Disinfection. *Environ. Sci.: Nano* **2019**, *6*, 2977−2985.

(46) Wang, H.; Yang, X.; Shao, W.; Chen, S.; Xie, J.; Zhang, X.; Wang, J.; Xie, Y. Ultrathin Black Phosphorus Nanosheets for Efficient Singlet Oxygen Generation. *J. Am. Chem. Soc.* **2015**, *137*, 11376−11382.

(47) Tao, W.; Zhu, X.; Yu, X.; Zeng, X.; Xiao, Q.; Zhang, X.; Ji, X.; Wang, X.; Shi, J.; Zhang, H.; Mei, L. Black Phosphorus Nanosheets as a Robust Delivery Platform for Cancer Theranostics. *Adv. Mater.* **2017**, *29*, 1603276−1603284.

(48) Yasaei, P.; Kumar, B.; Foroozan, T.; Wang, C.; Asadi, M.; Tuschel, D.; Indacochea, J. E.; Klie, R. F.; Salehi-Khojin, A. High-Quality Black Phosphorus Atomic Layers by Liquid-Phase Exfoliation. *Adv. Mater.* **2015**, *27*, 1887−1892.

(49) Korkut, S. E.; Küçükkeçeci, H.; Önder, M. Mesoporous Graphitic Carbon Nitride/Black Phosphorus/AgPd Alloy Nanoparticles Ternary Nanocomposite: A Highly Efficient Catalyst for the Methanolysis of Ammonia Borane. *ACS Appl. Mater. Inter.* **2020**, *12*, 8130−8139.

(50) Sun, Z.; Zhang, Y.; Yu, H.; Yan, C.; Liu, Y.; Hong, S.; Tao, H.; Robertson, A. W.; Wang, Z.; Pádua, A. A. H. New Solvent-Stabilized Few-Layer Black Phosphorus for Antibacterial Applications. *Nanoscale* **2018**, *10*, 12543−12553.

(51) Huang, Y.; Qiao, J.; He, K.; Bliznkov, S.; Sutter, E.; Chen, X.; Luo, D.; Meng, F.; Su, D.; Decker, J.; Ji, W.; Ruoff, R. S.; Sutter, P. Interaction of Black Phosphorus with Oxygen and Water. *Chem. Mater.* **2016**, *28*, 8330−8339.

(52) Wen, M.; Ouyang, J.; Wei, C. W.; Li, H.; Chen, W. S.; Liu, Y. N. Artificial Enzyme Catalyzed Cascade Reactions: Antitumor Immunotherapy Reinforced by NIR-II Light. *Angew. Chem. Int. Ed. Engl.* **2019**, *58*, 17425−17432.

(53) Yang, F.; Feng, Y.; Fan, X.; Zhang, M.; Wang, C.; Zhao, W.; Zhao, C. Biocompatible Graphene-Based Nanoagent with NIR and Magnetism Dual-Responses for Effective Bacterial Killing and Removal. *Colloid. Surface. B.* **2019**, *173*, 266−275.

(54) Wen, M.; Weinhart, M.; Lai, B.; Kizhakkedathu, J.; Brooks, D. E. Reversible Hemostatic Properties of Sulfabetaine/Quaternary Ammonium Modified Hyperbranched Polyglycerol. *Biomaterials* **2016**, *86*, 42−55.

(55) Richards, S.-J.; Isufi, K.; Wilkins, L. E.; Lipecki, J.; Fullam, E.; Gibson, M. I. Multivalent Antimicrobial Polymer Nanoparticles Target Mycobacteria and Gram-Negative Bacteria by Distinct Mechanisms. *Biomacromolecules* **2018**, *19*, 256−264.

(56) Liu, C.; Huang, Y.; Zhao, C.; Yang, F.; Qin, H.; Wang, Z. Cell Biophysical Characteristics of PPy-GNPs and Their Application in Photothermal Therapy of SKOV-3 Cell. *J. Nanopart. Res.* **2020**, *22*, 284.

(57) Liu, L.; Law, W.-C.; Yong, K.; Roy, I.; Ding, H.; Erogbogbo, F.; Zhang, X.; Prasad, P. N. Multimodal Imaging Probes Based on Gd-DOTA Conjugated Quantum Dot Nanomicelles. *Analyst* **2011**, *136*, 1881−1886.

(58) Ren, W.; Yan, Y.; Zeng, L.; Shi, Z.; Gong, A.; Schaaf, P.; Wang, D.; Zhao, J.; Zou, B.; Yu, H.; Chen, G.; Eric, M.; Wu, A. A Near Infrared Light Triggered Hydrogenated Black TiO_2 for Cancer Photothermal Therapy. *Adv. Healthcare Mater.* **2015**, *4*, 1526−1536.